Proceedings of the International Conference
Nanomaterials: Applications and Properties
Vol. 4 No 1, 01FPM06(4pp) (2015)

Edge States and Magnetization in Bernal-Stacked Trilayer Zigzag Graphene Nanoribbons

Juan Antonio Casao-Pérez*

Electronics Engineering and Communications Dpto. University of Zaragoza, María de Luna 3, 50018 Zaragoza Spain

(Received 30 June 2015; published online 29 August 2015)

We have used a tight-binding Hamiltonian of an ABA-stacked trilayer zigzag graphene nanoribbon with β-alignment edges to study the edge magnetizations. Firstly, in the neutral system we analyzed a magnetic state in which both edge magnetizations reach their maximum value; and is characterized by an intralayer ferromagnetic coupling between the magnetizations at opposite edges. The band structure and the location of the edge-state bands are calculated in order to understand the origins of the edge magnetizations. We have also introduced an electron doping so that the number of electrons in the ribbon unit cell is higher than in neutral case. As a consequence, we have obtained magnetization steps and charge accumulation at the edges of the sample, which are caused by the edge-state flat bands..

Keywords: Edge Magnetization, Trilayer Zigzag Graphene Nanoribbon.

PACS numbers: 75.75. + a, 75.90. + w

1. INTRODUCTION

Theoretical research on the electrical and magnetic properties of nanostructures based on monolayer [1-5], bilayer [6-8] and multilayer graphene [9-12] as well as experimental developments [13-15], have been carried out in order to use these properties in future applications. Special attention has been directed to analyzing the formation of the magnetic moments which are created by the localized edge states, and to how to control their magnitude. So, in monolayer graphene nanoribbons (MGNR) this magnitude has been (a) driven by the carrier density using gate doping [2]; (b) analyzed including nonlocal exchange effects [4] and (c) defined and controlled by the chirality angle and the chemical potential in chiral MGNR [3,5]. In bilayer zigzag graphene nanoribbons (BZGNR), the edge magnetization can be controlled by a transverse [7] or perpendicular [8] electric field applied to the ribbon. In multilayer structures, the density functional theory [10] and tight-binding Hamiltonians [11] have been used to study the dependence of the energy gaps and the edge magnetization on the type of edge alignment, the type of stacking (ABA or ABC) and the number of layers; furthermore, to understand how these properties are modified by an electric field perpendicular to the layers, and to see the unbalanced edge modes in gated trilayer GNR [12].

Here, we focus on the magnetic states of a Bernal stacked trilayer zigzag GNR with β alignment edge [10]. The intralayer and interlayer couplings between the edge moments can be ferromagnetic (FM) or antiferromagnetic (AF), and we study how they depend on doping. We work with a tight binding Hamiltonian that includes the effects of the interlayer hoppings γ_1 and γ_3 [15-17], the last one responsible for the trigonal warping. The Hubbard interaction is considered in the mean field approximation (MFA) [18], and only collinear solutions are studied.

2. THEORETICAL MODEL

In Figure 1, an ABA-stacked trilayer zigzag graphene nanoribbon (Bernal stacking TZGNR) with β alignment edges along x axis, is shown. It is formed with N_y (even) zigzag chains across the ribbon (y direction), so that the ribbon unit cell (ruc) contains $6N_y$ atoms. In this stacking, the central layer (layer 2 in Fig. 1) is a symmetry plane, thus the analysis becomes simpler. We describe this structure with a collinear single band Hubbard Hamiltonian in the MFA which includes the in-layer nearest neighbor hopping t; the in-layer next-nearest neighbor (nnn) hopping t', and we use $t' = 0.1t$ [19]; γ_1, the inter-layer coupling between atoms A1-B2 and B2-A3 which are one above the other; γ_3, the inter-layer coupling between atoms B1-A2 and A2-B3, and we use $\gamma_1 \cong \gamma_3 \cong 0.2t$ [15,16]; and U, the on-site Coulomb repulsion energy.

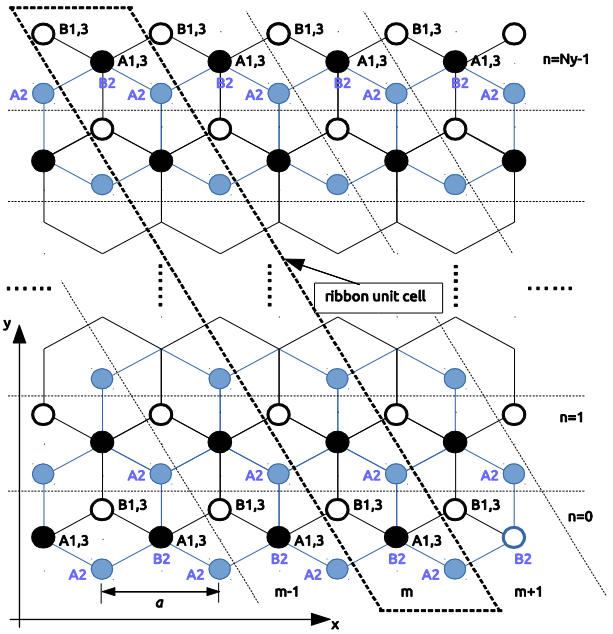

Fig. 1 – Bernal stacked trilayer zigzag graphene nanoribbon with β-alignment edges.

* casao@unizar.es

Because of the translation symmetry along the *x* axis, we transform the Hamiltonian *H* into *k*-space using $c^+_{lmn\sigma} = \left(1/\sqrt{N}\right)\cdot\sum_k e^{-ikma} c^+_{lkn\sigma}$, where *c* is the *a* or *b* operator and *a* is the lattice constant. $a^+_{lmn\sigma}(b^+_{lmn\sigma})$ are the creation operators of electrons respectively at layer *l* (*l* = 1,2,3), site *mn* with spin σ in sublattice $\eta = A$ ($\eta = B$); *m* = 1,..., *N*, with *N* specifying the length of the ribbon and *n* = 0, 1, ..., $N_y - 1$, with N_y the number of 6-atom elemental cells in the ruc. $n_{A,lkn,\sigma} = a^+_{lkn\sigma} a_{lkn\sigma}$ is the number operator and $\langle n_{\eta,lkn,\sigma}\rangle$ is its mean value, so $\langle n_{\eta,l,n,\sigma}\rangle = (1/N)\cdot\sum_k \langle n_{\eta,lkn,\sigma}\rangle$. Then, we can write $H = \sum_{k,\sigma} H_{k\sigma}$ [11,12,15-17], with

$$
\begin{aligned}
H_{k\sigma} = & -t \sum_{l=1,2,3} \sum_{n,\sigma} \left[a^+_{lkn\sigma}\left(b_{lkn-1\sigma} + e^{ika/2} 2\cos(ka/2)\; b_{lkn\sigma}\right) + h.c.\right] \\
& -t' \cdot \sum_{c=a,b} \sum_{l=1,2,3} \sum_{n,\sigma} \left[\left(e^{ika} + e^{-ika}\right)\; c^+_{lkn\sigma} c_{lkn\sigma} + \left(1 + e^{-ika}\right) c^+_{lkn\sigma} c_{lkn-1\sigma} \right. \\
& \left. + \left(1 + e^{ika}\right)\; c^+_{lkn\sigma} c_{lkn+1\sigma} \right] - \gamma_1 \sum_{l=1,3} \sum_{n,\sigma} \left(a^+_{lkn\sigma} b_{2kn\sigma} + h.c.\right) \\
& -\gamma_3 \sum_{l=1,3} \sum_{n,\sigma} \left[b^+_{lkn\sigma}\left(e^{-ika} a_{2kn\sigma} + e^{-ika/2} 2\cos(ka/2)\; a_{2kn+1\sigma}\right) + h.c.\right] \\
& +U \sum_{\eta=A,B} \sum_{l,n,\sigma} n_{\eta,lkn,\sigma} \cdot \langle n_{\eta,l,n,\bar{\sigma}}\rangle \\
& -(U/2)\cdot \sum_{\eta=A,B} \sum_{l,n} \langle n_{\eta,l,n\uparrow}\rangle \cdot \langle n_{\eta,l,n\downarrow}\rangle
\end{aligned}
$$

In order to solve $H_{k\sigma}$, an initial conjecture for $\langle n_{\eta,l,n,\sigma}\rangle$ is given. Then, the eigenenergies $E(k\nu\sigma)$ and eigenkets $|k\nu\sigma\rangle$ for the single particle Hamiltonian are computed; so that $H^{1p}_{k\sigma}\; |k\nu\sigma\rangle = E(k\nu\sigma)\cdot|k\nu\sigma\rangle$ and

$$
\begin{aligned}
|k\nu\sigma\rangle &= \sum_{\eta,l,n} \gamma_{\eta,l}(k\nu;n\sigma)\cdot|\eta lkn\sigma\rangle = \\
&= \sum_{l,n}\left[\alpha_l(k\nu;n\sigma)\cdot|Alkn\sigma\rangle + \beta_l(k\nu;n\sigma)\cdot|Blkn\sigma\rangle\right]
\end{aligned}
$$

with $\nu = 1,...,N_{at}$, $N_{at} = 6N_y$ is the number of atoms in the ruc; and the boundary conditions $\alpha_l(k\nu;N_y\sigma) = 0$, $\beta_l(k\nu;N_y\sigma) = 0$, $\alpha_l(k\nu;-1\sigma) = 0$ and $\beta_l(k\nu;-1\sigma) = 0$ for every *l, k, ν, σ*. Because of the time reversal symmetry we consider the interval $0 \le ka \le \pi$, and discretize it in 1601 points. At *T* = 0 K we have the self-consistent condition

$$
\begin{aligned}
\sum_{\eta,l,n}\left[\; \langle n_{\eta,l,n\uparrow}\rangle + \langle n_{\eta,l,n\downarrow}\rangle \;\right] &= n_{ruc} = \\
&= \sum_{\eta,l,n,\sigma} \int_0^{\pi} dk \cdot \sum_{\nu}^{occup.} \left|\; \gamma_{\eta,l}(k\nu;n\sigma)\;\right|^2
\end{aligned}
$$

where n_{ruc} is the number of electrons in the ruc; at half-filling $n_{ruc} = N_{at}$. So, for a given n_{ruc} we are filling the energy levels in increasing order of energy up to the self-consistent condition is satisfied. Then, new concentrations $\langle n_{\eta,l,n,\sigma}\rangle$ are computed, and a new Fermi level E_F is also computed, which is equal to the highest occupied energy level. This resolution procedure is repeated until convergence is reached.

3. RESULTS AND DISCUSSION

When $U = 0$ we find bands of zero energy for $2\pi/3 < ka \le \pi$, which correspond to the edge states [16]. When U is switched on, these flat bands give rise to a magnetic instability, and according to the Stoner criterion for itinerant magnetism a magnetic ground state is expected to be reached. We use $U = 1.2t$ [1,4]. Depending on the starting configuration for $\langle n_{\eta,l,n,\sigma}\rangle$, different types of solutions are obtained; and these solutions can be classified taking into account the intralayer and interlayer couplings between the edge spin polarizations [8]. Using this criterion, we have used five different types of starting conditions: 1) $m_{A20} = \langle n_{A20\uparrow}\rangle - \langle n_{A20\downarrow}\rangle > 0$, $m_{B2,Ny-1} > 0$, $m_{A1,3;0} > 0$ and $m_{B1,3;Ny-1} > 0$; that is, FM intralayer and FM interlayer; 2) $m_{A20} > 0$, $m_{B2,Ny-1} < 0$, $m_{A1,3;0} > 0$ and $m_{B1,3;Ny-1} < 0$, AF-FM; 3) $m_{A20} > 0$, $m_{B2,Ny-1} > 0$, $m_{A1,3;0} < 0$ and $m_{B1,3;Ny-1} < 0$, FM-AF; 4) $m_{A20} > 0$, $m_{B2,Ny-1} < 0$, $m_{A1,3;0} < 0$ and $m_{B1,3;Ny-1} > 0$, AF-AF; and 5) $\langle n_{\eta,l,n,\uparrow}\rangle = \langle n_{\eta,l,n,\downarrow}\rangle = (1/2)\cdot(n_{ruc}/N_{at})$, no magnetic. We have made a study of the spin moment of the six-atom elemental cell given by $m_n = \sum_{\eta,l}\langle n_{\eta l,n\uparrow}\rangle - \langle n_{\eta l,n\downarrow}\rangle$, *n* = 0, 1, ..., $N_y - 1$, as a function of the ribbon width. We have focused on the FM-FM solution, because in this solutions $m_n = 0$ and $m_n = N_{y-1}$ reach their maximum value.

First, we consider neutrality charge, so that $n_{ruc} = N_{at}$. Using the initial condition 1), the algorithm always converges to a FM-FM solution, and the results are shown in Figure 2. In Fig. 2a, the spin magnetic moments m_n at *n* = 0, 1, 2; $N_y - 1$, $N_y - 2$ and $N_y - 3$ are represented as a function of the ribbon width N_y (in units of μ_B). We clearly see that the edge magnetization saturates for low values of width, as it happens in monolayer zigzag GNR [5]. The fact that m_n, *n* = 0,1,2,... is, practically, equal to the corresponding ones at the opposite edge, is a consequence of the occupation and the location of the 6 bands of spin-up edge states, as discussed below. By using an ABA-trilayer ZGNR we have notably increased the spin magnetic moment of the cells at the edges. The reason is that the cell contains three atoms of the same type; two of them, by symmetry, contribute to the cell spin moment with the same magnitude, and the spin moment of the third one is aligned with the one of the two other previous atoms. We fix $N_y = 24$, and in Figure 2b we show the energy bands of the spin-up and spin-down states, where we clearly see the 6 bands of edge states of spin up, which are completely occupied; and the 6 bands of edge states of spin down, which are totally unoccupied (above the Fermi level, $E_F = 0.714$). As expected, these edge states arise for $2\pi/3 \le ka \le \pi$ [8,10,16,18]. In order to see the location of these edge bands with spin up, for every band ν and every 6-atom elemental cell position *n*, we have computed $\sum_{\eta,l,2\pi/3\le ka\le\pi}\left|\; \gamma_{\eta,l}(k\nu;n\uparrow)\;\right|^2$. From the results we deduce

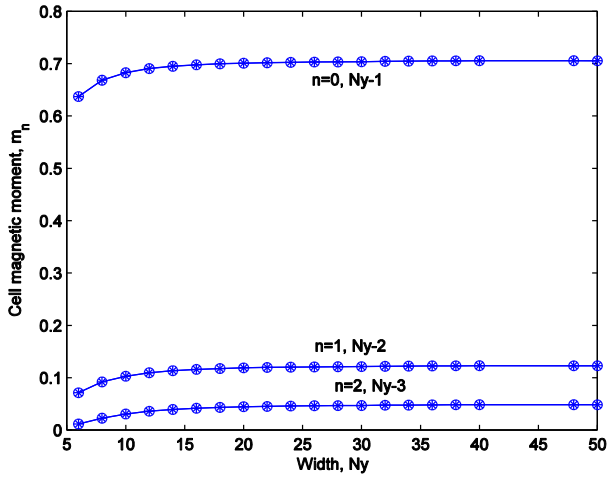

(a)

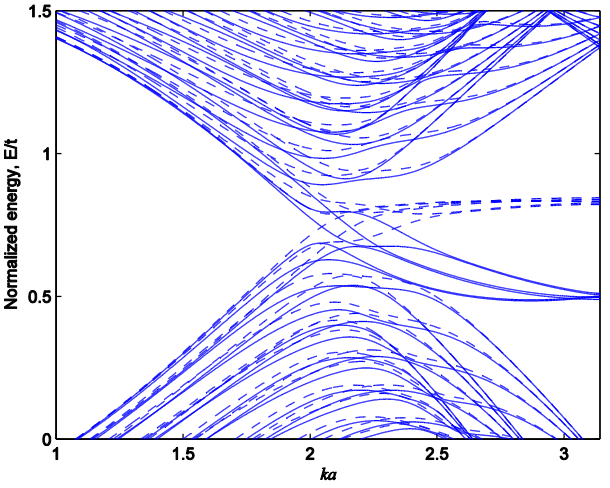

(b)

Fig. 2 – a) Spin magnetic moment at the edge cells $n = 0$, 1, 2 (*-) and $n = N_y - 1$, $N_y - 2$ and $N_y - 3$ (o-) in the FM-FM solution, as a function of width N_y. b) Energy bands $E_\uparrow$ (continuous line) and $E_\downarrow$ (dashed) in the FM-FM solution

that three bands are mainly localized at edge n=0 (say Right) and the other three are localized at the opposite edge $n = N_y - 1$ (say Left). Since all these bands are filled, the spin moment of cell n=0 will be, approximately, equal to that of cell $n = N_y - 1$; so we obtain $m_0 = 0.703 \cong m_{Ny-1}$. To m_0 contribute positively the atoms A2, A1 and A3 whereas m_{Ny-1} is built by the atoms B2, B1 and B3.

We now turn to the study of the edge magnetization as a function of doping, and as we explained above, we fix the number of electrons in the ribbon unit cell n_{ruc} and solve self-consistently in order to compute the Fermi level. The edge magnetization is defined by $m_{edge,\mu} = \sum m_n$, $\mu = R,\ L$; where from Fig. 2a, the three nearest cells are considered. We have used $N_y = 24$ and $n_{ruc} = N_{at} + \delta n_{ruc}$ with δn_{ruc} limited to $0.0 \le \delta n_{ruc} \le 2.0$; because beyond $\delta n_{ruc} = 2.0$ the edge magnetizations vanish. As a starting condition we use condition 1) (FM-FM), and the results are shown in Figure 3. Initially, at half filling, we have the six edge bands of spin up completely filled, and at very low doping levels ($\delta n_{ruc} \le 0.6$), both $m_{edge,\,R}$ and $m_{edge,\,L}$ decrease slowly as doping is increased. For $\delta n_{ruc} > 0.6$, we have found several regions in which either both $m_{edge,R}$ and $m_{edge,L}$ decrease uniformly with an increase of doping or they change abruptly, one of them reducing its value notably and the other increasing its value thought not so notably (transition regions). In the interval $0.6 < \delta n_{ruc} < 0.7$, an edge band with spin down and localized at $n = N_y - 1$ (Left) begins to occupy. By increasing the doping, because of the flat band, a great deal of states of the same energy needs to be occupied, producing a few states of spin down at edge $n = 0$ (Right) to be empty and that a left-edge spin-down band (LE↓B) becomes totally occupied. Therefore, $m_{edge,R}$ increases slightly its value while $m_{edge,L}$ reduces notably its value; that is, at $\delta n_{ruc} = 0.6$ $m_{edge,R} \cong m_{edge,L} = 0.750$ (in μ_B units) while at $\delta n_{ruc} = 0.7$ we have $m_{edge,R} = 0.782$ and $m_{edge,L} = 0.575$. The fact that this left edge band is full produces a left edge charge accumulation (LECA) (see Fig. 3). In $0.7 \le \delta n_{ruc} \le 1.05$, the LECA phenomena and the difference between $m_{edge,R}$ and $m_{edge,L}$, with $m_{edge,R} > m_{edge,L}$, are maintained and, because of new edge states of spin down in R and L edges are becoming filled, both magnetizations decrease slowly. The interval $1.05 < \delta n_{ruc} < 1.1$ is another short transition region, but now, two edge bands of spin down and localized at the right edge, are going to be occupied; which makes that at $\delta n_{ruc} = 1.1$ one LE↓B is filled and two right-edge spin down bands (RE↓B) are filled. Then, $m_{edge,R} < m_{edge,L}$ and there exists a right-edge charge accumulation (RECA). Again, from $\delta n_{ruc} = 1.1$ to 1.45, we have that, due to the fact that the populations of R-edge and L-edge states of spin down are increasing, both magnetizations reduce their value uniformly. Note that, at this doping level, we still have three edge bands of spin down completely unoccupied. For that reason, we could expect another transition region defined by $1.45 < \delta n_{ruc} < 1.60$, in which the system evolves from a state with two filled RE↓Bs and one filled LE↓B to a state with two filled LE↓Bs, one LE↓B partially occupied and two filled RE↓B. Therefore, in the next region of calmly variations ($1.60 \le \delta n_{ruc} \le 1.70$) we would have $m_{edge,R} > m_{edge,L}$ with $m_{edge,L}$ approaching zero, and charge accumulation in the left edge. Following this reasoning, by a very abrupt transition region

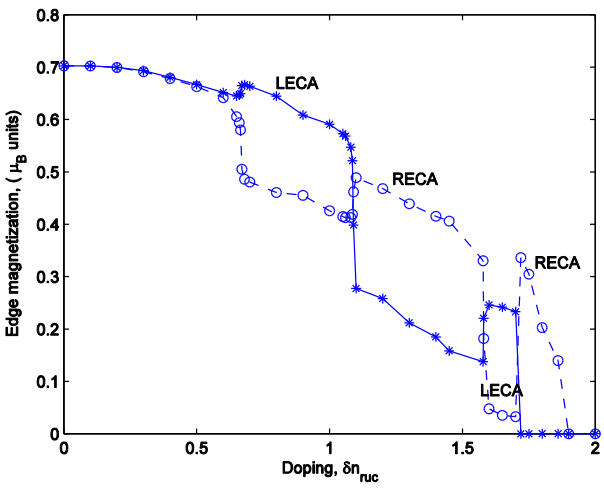

Fig. 3 – Edge magnetizations $m_{edge,R}$ (*-continuous-line) and $m_{edge,L}$ (o-dashed-line) as a function of doping δn_{ruc}.

($1.70 < \delta n_{ruc} < 1.72$) we would reach a zone ($1.72 \leq \delta n_{ruc} \leq 1.90$) with $m_{edge,R} \cong 0$, $m_{edge,L} > 0$ but rapidly going to zero as δn_{ruc} increases, and RECA. In this way, we would have four transition regions in which there are involved, respectively, one left-edge band, two right-edge bands, two left-edge bands and one right-edge band; all of them with down spin. However, in the range $1.45 < \delta n_{ruc} < 1.80$, our algorithm is not convergent; so that we are not sure of the results we have obtained in that interval. Finally, for $\delta n_{ruc} \geq 1.90$, $E_{\uparrow}(k) = E_{\downarrow}(k)$ and the system stops being magnetic, as it happens for monolayer graphene nanoribbons with chiral edges, when doping is increased [8]. So, for $n = 0,1,\ldots,N_y - 1$ we have $m_n = 0$.

AKNOWLEDGEMENTS

This work was supported by the Spanish Economy and Competitivity Minister through the project FIS2012-35719-C02-02.

REFERENCES

1. H. Castro Neto, F. Guinea, N.M.R. Peres, K.S. Novoselov, A.K. Geim, *Rev. Mod. Phys*. **81**, 109 (2009).
2. J. Jung, A.H. McDonald, *Phys. Rev B* **79**, 235433 (2009).
3. O.V. Yazyev, R.B. Capaz, S.G. Louie, *Phys. Rev. B* **84**, 115406 (2011).
4. Jeil. Jung, *Phys. Rev. B* **83**, 165415 (2011).
5. A.R. Carvalho, J.R. Warnes, C.H. Levenkopf, *Phys. Rev. B* **89**, 245444 (2014).
6. E. McCann, M. Koshino, *Rep. Prog. Phys*. **76**, 056503 (2013).
7. C. León, A. Latgé, *Phys. Rev. B* **88**, 245446 (2013).
8. Lihua Pan, Jin An, Yong-Jun Liu, *New J. Phys*. **15**, 043016 (2013).
9. K. Harigaya, *J. Phys.: Condens. Matter* **13**, 1295 (2001).
10. B. Sahu, Hongki Min, S.K. Banerjee, *Phys. Rev. B* **82**, 115426 (2010).
11. J. Jung, F. Zhang, Zhenhua Qiao, A. H. MacDonald, *Phys. Rev. B* **84**, 075418 (2011).
12. Xiao Li, Z. Qiao, J. Jung, Qian Niu, *Phys. Rev. B* **85**, 201404 (2012).
13. Chenggang Tao, et al., *Nature Phys.* **7**, 616 (2011).
14. G.Z. Magda, Xiaozyhan Jia, I. Hagymási, P. Vancsó, Z. Osváth., P. Nemes-Incze, Chanyong Hwang, L.P. Biró, L. Tapasztó, *Nature* **514**, 608 (2014).
15. C. Coletti, S. Forti, A. Principi, K.V. Emtsev, A.A. Zakharov, K.M. Daniels, B.K. Daas, M.V.S. Chandrashekhar, T. Ouisse, D. Chausende, A.H. MacDonal, M. Polini, U. Starke, *Phys. Rev. B* **88**, 155439 (2013).
16. E.V. Castro, N.M.R. Peres, J.M.B. Lopes dos Santos, *Europhys. Lett.* **84**, 17001 (2008).
17. A. A. Avetisyan, B. Partoens, F. M. Peeters, *Phys. Rev. B* **81**, 115432 (2010).
18. M.P. Lima, A.J.R. da Silva, A. Fazzio, *Phys. Rev. B* **81**, 045430 (2010).
19. K. Sasaki, S. Murakami, R. Saito, *Appl. Phys. Lett.* **88**, 113110 (2006).